EUROPEAN ORGANIZATION FOR NUCLEAR RESEARCH

CERN/EP 82-55
10 May 1982

A HIGH LUMINOSITY SPECTROMETER FOR DEEP INELASTIC MUON SCATTERING EXPERIMENTS

D. Bollini, P.L. Frabetti, G. Heiman, G. Laurenti, L. Monari and F.L. Navarria.
Istituto di Fisica dell'Università and INFN, Bologna, Italy

A.C. Benvenuti[1], M. Bozzo[2], R. Brun, H. Gennow[3], M. Goossens, R. Kopp, F. Nanni, F. Navach[4], L. Piemontese, C. Rubbia and D. Schinzel
CERN, European Organization for Nuclear Research, Geneva, Switzerland

J. Cvach, I.A. Golutvin, I.M. Ivanchenko, V.S. Khabarov, Y.T. Kiryushin, V.S. Kisselev, V.G. Krivokhizhin, V.V. Kukhtin W.D. Nowak, I.A. Savin, D.A. Smolin, L.V. Svetov, G. Vesztergombi A.V. Vishnevsky, A.G. Volodko, J. Zacek, A.V. Zarubin and Y.L. Zlobin
Joint Institute for Nuclear Research, Dubna, USSR

D.Jamnik[5], U. Meyer-Berkhout, A. Staude, K.M. Teichert, R. Tirler, R. Voss and C. Zupancic
Sektion Physik der Universität, Munich, FRG

and

J. Feltesse, J.C. Michau, A. Milsztajn, B. Pichard, J.F. Renardy, B. Rothan, Y. Sacquin, G. Smadja, P. Verrecchia and M. Virchaux
CEN, Saclay, France.

Submitted to Nuclear Instruments and Methods in Physics Research

---

1) Now at the Istituto Nazionale di Fisica Nucleare, Bologna Italy.
2) Now at Istituto Nazionale di Fisica Nucleare, Genova, Italy
3) Now at DESY, Hamburg, FRG
4) Now at the University of Bari, Italy
5) On leave from the E. Kardelj University and the J. Stefan Institute, Ljubljana, Yougoslavia

0014P/jr

- CONTENTS -

1. INTRODUCTION

The classic experiments of the SLAC-MIT group [1] on inclusive electron scattering had a fundamental influence on the understanding of the structure of the nucleon. The increased energy and the high quality of the muon beam constructed at the CERN SPS offer the possibility of probing the nucleon structure at much smaller distances. In these experiments the interaction of the virtual photon with the charged constituents of the nucleon can be studied in function of the photon energy, mass and polarization by varying the energy and angle of the scattered muon.

The weak interaction properties of the muon can be studied through the interference between the photon propagator and the neutral current component of the weak interaction [2]. The interference can be measured by comparing the cross sections of left-handed and right-handed muons as well as the cross sections of muons of opposite charge. The magnitude of the effect depends linearly on the four-momentum transfer (Q^2) and is expected to be of the order of 10^{-4} Q^2 (GeV^2). The longitudinal muon polarization can be varied by changing the relative momentum of the parent and daughter particles in the beam.

The muon beam can also be used to study the production of heavy vector states (J/ψ,T), charmed particles and heavy leptons through their leptonic decay modes.

In view of the importance of these investigations we have built a spectrometer which was designed to study the inclusive Deep Inelastic Scattering (DIS) process on hydrogen, deuterium and carbon

$$\mu^{\pm} + p(d,C) \rightarrow \mu^{\pm} + \text{anything} \qquad (1)$$

with high statistics and good resolution up to the highest energies and Q^2 available at the CERN SPS.

Clearly a large luminosity of the detector is essential in order to overcome the $1/Q^4$ reduction of the cross sections and to make statistically meaningful measurements up to $Q^2 \sim 300$ GeV^2 with the

relatively feeble muon fluxes. Radiative losses, which in the case of electron scattering are determinant for the choice of a very short ($\sim$ 5 cm) target are no longer relevant since the effect is lessened by the factor $(m_e/m_\mu)^2 \sim 2.3 \times 10^{-5}$ and hence an extended target can be used.

2. PRINCIPLE OF THE SPECTROMETER

The apparatus (fig. 1) consists of a 50 m long torus of magnetized iron with a central hole where the targets are located. The torus is magnetized to saturation and the magnetic field inside the iron is to a good approximation constant and equal to two Tesla. All particles which are produced in a DIS process and reach the torus are filtered out after several collision lengths, except for the muons. Most often only the scattered muon survives and from this point on, the spectrometer is a single-particle detector.

The principle of the spectrometer is shown in fig. 2. For clarity, we neglect in the discussion the effects of energy loss and of multiple scattering inside the iron. Muons of the same charge as the incident beam are focussed by the magnetic field in such a way as to perform periodical oscillations inside the magnetized iron. The oscillations, which are symmetric with respect to the main axis of the spectrometer, retain muons permanently trapped inside the magnetized iron provided enough space is available inside the torus. Periodic oscillations can be characterized by a peak amplitude Δ and a half wave-length $\lambda_{1/2}$ which are related to the kinematics of the DIS process as follows:

$$\lambda_{1/2} = 6.66\ p_T/B \tag{2a}$$

$$\Delta = \frac{M}{0.3B} \cdot \frac{Q^2}{Q^2_{max}} = \frac{M}{0.3B} \cdot xy \tag{2b}$$

where:

- p_T is the transverse momentum of the scattered muon, $p_T = p_\mu \sin\theta_\mu$ in GeV,
- B is the magnetic field inside the torus in Tesla,
- M is the nucleon mass,

- Q^2, Q^2_{max} are the value and the maximum permissible value of the four-momentum transfer: $Q^2 = 2E_0E_\mu (1-\cos \theta_\mu)$, with E_0 and E_μ respectively the incident and scattered muon energy, $Q^2_{max} = 2ME_0$, $\nu = E_0 - E_\mu$, and x and y are the usual scaling variables, $x = Q^2/(2M\nu)$ and $y = \nu/E_0$.
- Δ and $\lambda_{1/2}$ are given in meters.

Some of these kinematical relationships are illustrated in fig. 3.

The toroidal structure of the spectrometer has the following useful properties :

(a) All scattered muons with Δ smaller than the difference between the outer and inner radius of the torus are confined inside the torus, irrespective of the emission angle and of the beam momentum.

(b) The peak displacement Δ is proportional to Q^2/Q^2_{max}. Direct event selection according to the fractional value of the maximum four-momentum transfer can be easily performed with a simple set of ring counters located periodically within the structure.

(c) The azimuthal symmetry of the spectrometer greatly reduces the sensitivity of the cross section measurements to variations of the beam phase space.

Energy losses introduce a correction term in the relation between Q^2 and Δ but do not modify these features in a major way.

3. GENERAL DESCRIPTION OF THE APPARATUS

The general layout of the apparatus is shown in fig 1(a). The spectrometer is subdivided into ten identical supermodules each 5.25 m long, separated by 40 to 60 cm long free sections. The free sections allow sufficient space for the return paths of the coils, the filling system of the hydrogen/deuterium target and a beam hodoscope. Each supermodule (fig. 1(b)) consists of:

(a) a separate hydrogen, deuterium or carbon target,
(b) the magnetized iron and the coil,
(c) Multiwire Proportional Chambers (MWPC) and Trigger Counters (TC) to determine the muon trajectory inside the iron.

The components are mounted rigidly inside the supermodules which can be moved sideways on rails as individual units. The iron in each supermodule is subdivided into eight units spaced 10 or 20 cm apart to accommodate the wire chambers and the trigger counters.

In each supermodule there are eight MWPC planes alternatively measuring X and Y coordinates of the tracks and two planes of TC's. The TC planes detect the presence of a scattered muon inside the iron toroid with a high efficiency and good timing.

A set of three beam defining hodoscopes (HOD5 to HOD7) with a mosaic structure designed to withstand fluxes of up to 10^9 muons/burst are installed in the spectrometer. They are used to correlate the beam muon which initiated the trigger with the momentum defining hodoscopes installed in the beam line and with the target section where the interaction occurred. Furthermore, they are used to monitor the beam flux and the steering of the beam through the apparatus which is very important given the length of the spectrometer. The first of these hodoscopes is also used as "beam counter" in the trigger logic.

The apparatus is shielded against the beam halo muons by a veto system made of scintillation counters ("halo wall"). Because almost every halo muon entering the apparatus is trapped in the magnetic field of the spectrometer and can generate a trigger, the efficiency of this system and its rejection power against the halo should be very high in order to eliminate one of the main sources of spurious triggers and a potential background to DIS events.

4. ELEMENTS OF THE APPARATUS

4.1 Layout of the beam and its characteristics

The CERN SPS muon beam line M2 is schematically shown in fig. 4(a) and has been described elsewhere, [3]. Here we recall its salient properties.

The momentum band of the beam is ± 4% (r.m.s.) of the nominal value which can be as high as 300 GeV/c. A set of beam hodoscopes [4] in front of and behind the last bending magnet of the beam spectrometer stage (Beam Momentum Station, BMS) provide an individual muon momentum determination with a precision of 0.5%.

The back end section of the beam has magnetic collimators which can be used to minimize the ratio of the beam halo to the beam intensity. At our spectrometer the halo has two main components one from the front of the spectrometer (about 10% of the incoming beam) and the other from underground (about 1%). The origin of the latter component is in the hadron absorber region.

At the entrance of our detector the beam is restored on axis, albeit with a lateral displacement of 12 cm, see fig. 4(b), by a system of magnets which compensate the horizontal bend introduced by the EMC spectrometer [5]. The beam profile has a shape which is approximately a two dimensional gaussian with $\sigma_x \simeq \sigma_y = 2$ cm. The beam divergencies in the horizontal and vertical planes are approximately equal to 0.3 mrad, and 0.6 mrad respectively.

For positive muons of 120, 200 and 280 GeV the muon yields over a circular region with 8 cm diameter are respectively equal to $3.8.10^{-5}$, $1.4.10^{-5}$ and $1.8.10^{-6}$ per 400 GeV proton incident on a 50 cm beryllium target. The intensities of the negative muons are about three times smaller. In practice beam intensities of about 2.10^7 muons in 1.5 s long bursts were used.

Muons originate mainly from two-body pion and kaon decays and have a longitudinal polarization which depends on the ratio of daughter to parent energy which can be changed by varying the setting of the hadron beam transport line elements relative to those of the muon line. E.g. for a μ^+ coming from π^+ decay the longitudinal polarization is [6]

$$P_{L,\mu^+} = - \frac{u - m_\mu^2/m_\pi^2(1-u)}{u + m_\mu^2/m_\pi^2(1-u)} \qquad (3)$$

with

$$u = \frac{E_\mu/E_\pi - m_\mu^2/m_\pi^2}{1 - m_\mu^2/m_\pi^2} \quad . \qquad (4)$$

Fig. 5 shows the longitudinal polarization of the positive muon beam in function of the ratio of average energies, $\langle E_\mu \rangle / \langle E_\pi \rangle$. The simple formula, eq. (3), compares well with the predictions of a Monte-Carlo calculation [7] which simulates fully the beam transport elements and the particle production spectra. The longitudinal polarization of the M2 muon beam was measured for various settings of the positive beam by detecting the positrons from muon decays [8]. The results of the measurements are also plotted in fig. 5 and within the rather large errors are found to be in good agreement with the calculations.

It has to be noted that a large negative μ^+ longitudinal polarization is obtained by working with similar muon and pion momentum bands, $\langle E_\mu \rangle / \langle E_\pi \rangle > 0.9$, and corresponds therefore to the maximum muon flux at each beam energy. A positive polarization on the other hand can be obtained only by setting $\langle E_\pi \rangle$ as high as possible in order to obtain $\langle E_\mu \rangle / \langle E_\pi \rangle < 0.7$ and this is possible only at the expense of a considerable decrease in muon flux for fixed muon energy: with 400 GeV protons and $\langle E_\mu \rangle = 200$ GeV there is a factor 10 decrease in going from $\langle E_\pi \rangle = 220$ GeV to $\langle E_\pi \rangle = 300$ GeV and the polarization varies from −0.8 to +0.2.

4.2 Spectrometer magnet

The magnet of the toroidal spectrometer consists of ten identical supermodules representing independent magnetic units each with its own core, coil and feeder. The core modules are made of four 11 ± 0.5 cm thick discs mounted on a I profile girder. They are cut and machined from plates of low carbon standard USSR rolled steel of type 08 (carbon content is between 0.06 and 0.1%). There are 1.3 ± 0.3 cm air gaps between the

adjacent discs for installation of additional detectors. The steel thickness (44.0 cm) and total thickness (48.3 cm) are constant for all modules. The discs have an outer and inner diameter of 275 and 50 cm, respectively and are welded into a module with the help of four stainless steel plates, 2 cm thick, placed at the end of each of the 45° diagonals. Two lifting lugs and two supporting legs made of standard steel are welded to the plates.

The magnet coil is made from four sets of six copper conductors placed in the hole of the supermodule close to the inner surface of the steel discs at the 45° diagonals. Each conductor has a cross section of 2 x 2.5 cm^2 with an inner hole for water cooling. The conductors are parallel to the spectrometer axis and bent by 90° at its ends. Each conductor is fed by 2500 A direct current, the supermodules are fed in series and the return current flows at 275 cm from the axis.

The magnetic properties of the steel have been measured using steel samples cut from each original rolled plate. The magnetic induction has been measured for 435 samples at 5 fixed values of the magnetic field. The mean values of B are shown in table 1. At the maximum field the variance of the mean induction (σ_B) is less than 0.5%.

TABLE 1

H, Oersted	3	10	50	100	300
B, Tesla	0.557	1.273	1.610	1.730	2.002
σ_B	0.048	0.074	0.017	0.010	0.009

Our spectrometer is long compared to its diameter and, to a good approximation, uniform along its axis. The three-dimensional aspects of the magnetic field are of minor importance for the momentum determination of scattered muons originating nearly uniformily from the long target. Therefore, we use a simplified two-dimensional model of the spectrometer for the calculation of the magnetic induction $\vec{B}(r,\phi)$ as a function of the radius r and the azimuthal angle ϕ. The calculation has been performed with the program POISSON originally developed at LBL and adapted to our purposes [9].

The magnetic induction is essentially tangential to circles centered on the axis and varies from ca. 2.1 T at the inner edge of the iron to ca. 1.8 T at the outer edge. The field leakage into the supports introduces a small angular dependence of the absolute value of B and a normal component which is less than 0.02 T except in the vicinity of the supports where it reaches up to 0.15 T. The magnetic induction in the central hole is smaller than 0.01 T up to a radius of 13 cm and reaches its highest value of ca. 0.05 T at the surface of the coils.

In the reconstruction program the map $\vec{B}(r,\phi)$ is calculated by a ficticious currents method which introduces further approximations beyond the assumption of the two-dimensional field. However, this method is more flexible for the parametrization of any measured deviation of the real field $\vec{B}(r,\phi)$ from its previously calculated value.

The magnetic flux through the torus has been measured with induction coils wound around different sections of a supermodule and around several entire supermodules. The observed variation of the flux in the iron along the spectrometer axis is consistent with the known variation in the magnetic permeability of the plates. The absolute value and ϕ-dependence of the measured flux agree with the results of the POISSON program to better than 1%. By a suitable choice of fictitious currents one can obtain a field map $\vec{B}(r,\phi)$ which reproduces the measured fluxes to better than 0.3%.

The absolute value of the magnetic field has been checked to better than 1% with the help of particles of known energies (120 and 200 GeV) deflected directly into the iron of the spectrometer.

During the experiment the spectrometer field was controlled locally by Hall probes tightly fitted into the iron, and the field was kept on a given hysteresis loop by computer control of the current. In addition the voltage drop across each supermodule was monitored to guard against undetected coil short circuits. These measures provided a stability and reproducibility of the field over long periods to better than 5.10^{-4}.

4.3 Proportional chambers

Each of the 80 MWPC planes consists of two identical chambers with dimensions 300 x 150 cm^2. Details of a chamber structure are shown in fig. 6. The chamber is constructed of two self supporting panels, two frames woven with 20 μm diameter gold plated tungsten wires and printed circuit boards.

The panels are 20 mm thick and are made of a plastic material with a honeycomb structure glued between two 0.5 mm fiber glass skins. They are silver painted on the inner side which is used as a high voltage negative plane. The gap between the wire plane and the negative h.v. plane is 7 mm. There is a square cut at the center of one of the long sides of the panel corresponding to the central hole of the magnet. Four equidistant spacers are inserted between the panels to keep the chamber gap uniform over the whole surface. The wires, stretched along the 300 cm side, are supported by nylon strings every $\sim$ 60 cm and soldered to the printed circuit boards. The wire spacing is 2 mm but the wires are connected in pairs so that the readout takes place every 4 mm. This accuracy is sufficient since magnetic deflections are quite large and the final accuracy is dominated by multiple Coulomb scattering. In the region of the central hole the wires are connected outside the chamber with flat cables.

A gas mixture of 68.7% argon, 28% isobutane, 3% methylal and 0.3% freon is used to flush the chambers and the flux is automatically controlled by thermic flux meters which guarantee a stability of 1%.

The readout electronics is of two different types F6 [10] and LRS [11] with comparable performances, which where designed in accordance to a common set of specifications.

Each chamber has 11 electronic cards connected to it. A card contains 32 channels each consisting of an amplifier with an input impedance of 220 Ω followed by two parallel monostables with equal delays of 470 ± 10 ns. Each monostable is addressed in turn by a flip-flop in order to reduce the channel inefficiency due to the dead time. At the rate of 10^5 signals per channel this inefficiency was $2.5\ 10^{-3}$. The trailing edge of the monostables gated by the strobe signal (first level trigger) causes the transmission of the information from the chamber to the first buffer, (see fig. 7). The information is stored there until a signal from the second level trigger either clears this buffer (abort) or transfers the information into the second buffer (accept) which is finally read by the computer via a CAMAC interface. The main difference between the two electronic systems is that for LRS the read out is serial up to 1024 channels while for F6 each group of 16 channels is addressed separately. In both cases the input threshold is set at 5 μA.

A broad efficiency plateau of a few hundred volts has been obtained for all 160 chambers. The spread in the beginning of the plateau is less than 100 volts. Typical delay curves obtained by varying the timing of the strobes are shown in fig. 8.

Before installation in the spectrometer the MWPCs were thoroughly tested either with a Ru^{106} radioactive source or with cosmic rays [12]. The overall system of MWPCs and associated electronics have given an excellent performance during long periods of data taking. The rate of broken wires has been typically 3 out of 112640 per year, while the number of noisy and dead channels has been 20 out of 56320 per two months of operation.

4.4 Trigger counters

The scintillation trigger counters were designed according to the following criteria:

- azimuthal symmetry around the target,
- Q^2 - selectivity by radial subdivision,
- good timing resolution,
- modularity and simplicity of construction.

A trigger counter plane is made of two identical liquid scintillator counters as shown in fig. 9. Each counter consists of an aluminium container subdivided into seven half rings of equal width (142 mm) and thickness (30mm) by spacer bars 8 mm thick (causing a dead area of about 5%). Each half ring is connected at the extremities to a straight light guide box ending in a semiadiabatic plexiglass light pipe. The half rings are filled with liquid scintillator and the light guide box with non-scintillating mineral oil, the two liquids being separated by a plexiglass window. The whole container is made oil tight by using fluorocarbon rubber.

The scintillator used, NE235, has the following characteristics: 40% light output as compared to anthracene, light attenuation lenght greater than 4 m and a main decay time of 4 ns.

To guide the light through the counter (the longest light path being approximately 6 m) all inner surfaces of the container are covered with a thin layer of aluminized teflon. The teflon has an index of refraction of 1.35 as compared to 1.47 for the liquid scintillator thus giving total internal reflection of light at the boundary with a critical angle of 66° [13].

Each ring is seen by 2 two-inch photomultipliers (PM) EMI 9814KB whose outputs after discrimination are sent to a mean timer. The PMs are shielded against the rather high fringe fields of the spectrometer by iron shields in addition to the mu-metal shielding in the base assembly.

Counters of these dimensions are delicate because of the large dynamic range required and the small amount of photoelectrons produced by minimum ionizing particles. The light seen by any one of the PMs depends strongly on its origin inside the ring; the ratio of average light intensities seen by the 2 PMs varies for all rings from 1 : 1 to about 1 : 6 depending on whether the light originates at the center of the ring or at its extremities. A muon traversing the counter at the most unfavorable position gives rise to 4-5 photoelectrons on the average in the far phototube.

To obtain maximum efficiency, the discrimator thresholds are set so that about 50% of the one-photoelectron pulses are accepted. The resulting efficiency is better than 95% for the most unfavorable position and better than 99% on the average.

Operating these counters with relatively low thresholds in the muon spectrometer gives rise to another problem: muons in the hundred GeV range have an energy loss distribution with a strong high loss tail (due to bremsstrahlung and nuclear interactions) and are sometimes accompanied by the hadronic shower from the deep inelastic scattering causing very high pulses. A high pulse has a fluctuating tail due to late arriving photons which may induce the refiring of the discrimator ("afterpulsing"). This leads to an undesirable increase of the random triggering rate. It has been found that the afterpulsing could be reduced to an insignificant level without impairing the timing characteristics of the counter by a passive pulse shaping network at the anode of the phototube. The network consists of a 3 ns long 50 Ω clipping cable terminated by 6 Ω and an RC integrating element (τ = 4ns) which shapes the signal to a resulting width of about 10 ns (time over threshold) with a small (25%) overshoot. The time resolution of the counter after the mean timer is $\sigma < 1$ ns for a fixed impact point; there is a time slewing of about 1 ns between a central hit and a hit at the extremities.

The gain of the phototubes and the stability of the triggering system was monitored by Light Emitting Diodes, using the dynode of each phototube connected to an analog to digital converter.

4.5 Beam hodoscopes

The hodoscope system consists of 7 planes of scintillation counters distributed over a total distance of about 240 m. The first four hodoscopes provide the energy measurement of the muon beam (BMS) with a relative accuracy of ±.5%. They consist of 64 elements arranged in a finger like structure with 5 mm width and are described elsewhere [4]. Hodoscopes 5, 6 and 7 have a mosaic structure adapted to the azimuthal symmetry of the spectrometer and measure the muon trajectory in the

target. Each of these hodoscopes, see fig. 10, consists of 72 elements made of 2 cm thick Pilot U scintillator arranged into six polygonal rings which cover an octagonal area 20 cm wide. The outer eight elements are used to study the halo component close to the beam.

The size of the individual elements is determined by the beam profile and the requirement that the counting rate be not higher than 3% of the total beam intensity. Thus the spatial resolution varies from 2 mm (RMS) in the beam center to 9 mm (RMS) at the outer part. This is the same order of magnitude as the average spatial displacement of a 100 GeV muon through 15 m of carbon due to multiple scattering.

The mechanical structure of the hodoscopes consists of 6 armco-iron disks with a central hole of 16 cm diameter for the beam interspersed with 5 planes of scintillator and air lightguide "sandwiches". The iron plates give the necessary mechanical stability and together with a .5 mm mu-metal cylinder screen each PM from the magnetic stray field (up to 750 Oersted) generated by the magnet return coils.

The pulse from each element of the hodoscopes is sent after a two level discrimination [4] and proper gating by the experiment trigger to a system of Time to Digital Converters (TDC) which provides a time resolution of better than 180 psec. The relative timing of the hodoscope elements were adjusted by triggering on the beam itself in special runs during regular data taking. The stability of the TDC system was also periodically checked.

The overall efficiency for correctly assigning the beam energy to the incoming muon was found to be $\sim$ 85%. The inefficiency of the system was partly due to the sharing of the BMS with the EMC experiment ($\sim$ 2%), to inefficiency in the pattern recognition ($\sim$ 7%) and to ambiguities between muons too close in time to be separated ($\sim$ 6%).

4.6 Antihalo system

The main element of the halo wall (see Figs. 1 and 11) is an iron tank 2.9 x 2.9 x 0.1 m^3, internally coated with aluminized teflon and filled with liquid scintillator. A central hole of 0.5 x 0.5 m^2 matching the

insensitive region of the MWPC downstream, is provided for the beam. The light is collected with good time resolution by 24 five-inch (58 DVP) PMs distributed over the largest side of the tank, which are combined into four quadrants: the signals from all PMs belonging to the same quadrant are added linearly and discriminated. The quadrant signals are then OR'ed together to provide the TANK signal. The tank hole is covered by a system of 12 wedge-shaped counters (IRIS) which are placed concentrically around the beam axis to leave a central aperture whose diameter could be adjusted remotely.

Due to the presence of some halo component far away from the beam axis but converging towards the apparatus and entering from its sides, the surface of the halo wall was extended by adding the "down" and "side" components. The total surface of the halo wall is therefore $\sim$ 22 m^2, and its counting rate ranges from 15% to 20% of the beam intensity, according to beam energy and polarity. This counting rate is higher than the halo rate due to the contribution of small pulses ("soft component"). The signals from the halo wall are shaped and grouped into four first level ORs: IRIS, TANK, DOWN and SIDE. Particular care is taken to ensure that the operation of the halo wall is not affected by dead time: LRS 621CL discriminators are used in a mode that OR'es the input signal to the shaped output (burst guard mode). As a second precaution, two outputs from the same elements (e.g. TANK) are OR'ed together with a relative delay of $\sim$ 20 ns, in order to increase the pulse width without creating a dead time, thus covering the dead time of the discriminator.

A pulse width of about 60 ns is chosen for the halo signal in order to reject the halo triggers to the level of 10^{-5}.

The halo anticoincidence reduces the lifetime for data taking by $\sim$ 20% in normal running conditions. Since the apparatus is meant to measure absolute cross sections, we make sure that every beam μ which can trigger the apparatus is counted, and vice-versa. For this reason the halo condition on our trigger is applied by requiring a "beam $\cdot$ $\overline{\text{halo}}$" coincidence which is then used as the "beam signal" both for counting and for triggering.

5. TRIGGER

5.1 Distributed trigger logic

A constraint in designing the trigger is that it should collect the interactions wherever they occur along the 40 meter long target with as uniform conditions as possible. Another strong constraint is given by the delay time of each channel in the MWPCs electronics ($\sim$ 470 ns) which is the maximum available time to generate a trigger and to distribute the strobes to the electronics on the MWPCs.

With these considerations in mind the trigger logic, shown in fig. 12, was designed to be simple and modular so that it could be easily reproduced in several logic stations located along the detector.

The transmission of the information from the trigger elements to the logic stations is achieved with a system of 50 Ω copper coaxial lines (highways) which have a transmission speed close to the speed of light ($\beta = 0.99$) and therefore allow to keep synchronization along the detector of the electronic information and the muon that generated it.

In more detail, the output of the photomultipliers viewing each individual half ring of a trigger counter plane is sent after discrimination to a meantimer which produces a signal (ring) independent in time from the impact point of the muon on the counter. The ring signals from all the half rings in a trigger plane are collected by a Multiple And Or unit (MAO) which can be remotely controlled to produce the desired ring configuration for the output pulse (plane signal).

Each plane signal is then injected into its own highway line and distributed along the detector to the remotely controlled logic stations (programmable coincidences and strobe fan-outs).

In addition to the plane highways there are several other highway lines which run along the full length of the detector:

- the beam highway which carries the beam signal after the veto from the antihalo system (beam $\cdot$ $\overline{\text{halo}}$),

- the strobe line which brings the information on the occurrence of a trigger,
- the reset line which is used to restart the logic stations after each trigger,
- the spill gate line which inhibits the logic stations outside the beam spill.

The logic stations are located at each supermodule; only the first seven are used to generate the trigger the others just relay the strobe signal to the MWPCs. The plane signals from six consecutive trigger planes located at any of the seven logic stations and downstream of it are picked up from the highway lines, appropriately delayed and reshaped with time over threshold discriminators and sent to the logic station which applies the chosen trigger requirements.

The standard trigger condition for data taking was the coincidence of four consecutive trigger planes and the beam $\cdot \overline{\text{halo}}$ signals at any logic station.

The timing of the signals at each logic station was kept within $\pm$ 2 ns and the timing between the passage of the muon and the generation of the trigger was independent of the logic station within $\pm$ 1 ns. This relative timing of the various logic stations is important because the occurrence of the trigger must be linked in time with beam hodoscopes (beam momentum station) which allow to assign the correct beam energy to the event.

Upon the occurrence of a trigger in a logic unit a strobe is generated directly for the MWPCs associated with that logic station, it is injected in the strobe highway and the logic unit is blocked to prevent generating other triggers until the current one has been read by the data acquisition system.

The other stations, upstream and downstream of the trigger origin, relay the strobe signal from the strobe line to the respective MWPCs and are blocked. The strobe signal is also picked up downstream of the last

injection point into the strobe highway and sent to the counting room to provide a trigger timing independent of the position of the trigger along the detector.

Since the trigger components are located in the experimental area and are inaccessible during data taking, a remote control system (SATAN) [14] has been developed to communicate with all the units involved in the trigger. Furthermore a great redundancy was built into the monitoring system to permit the detection of faulty components quickly.

Each of the half-ring signals, and all the signals used as inputs to each logic station are brought into the counting room using cable lengths such as to compensate for the muon transit time so that the information from the various parts of the detector is available in time in the counting room for further analysis of the trigger (second level logic).

To provide a good redundancy in the off line validation of the trigger by the reconstructed track, the half ring signals and the plane signals for the full plane, the half plane left and the half plane right are also recorded on Pattern Units (PU) together with the pattern of the logic units which generated a trigger. Furthermore, all the inputs to each logic station are recorded on PU and their timing measured with TDCs.

In the off-line analysis an event is considered good only if the reconstructed track satisfies the trigger requirement of at least one of the logic stations which generated the trigger and the ring crossings deduced from the reconstructed track match the pattern recorded at data taking.

5.2 Trigger rates

The Q^2 selectivity of the trigger is obtained by using different ring configurations in the definition of the plane signals thus requiring the muon to be above a given sagitta in the toroids and hence have a Q^2 above the corresponding cut-off. The length of the trigger (in number of trigger counter planes) corresponds to a cut-off on the transverse momentum

of the scattered muon. In principle short trigger lengths are preferred since they allow to investigate a wider Q^2-x domain and provide a larger trigger redundancy for long tracks.

In practice the trigger length is determined by the trigger rate which the data acquisition can service since short triggers are easily satisfied by the punch through of hadronic showers generated by low Q^2 interactions. For standard data taking a trigger length of four planes is chosen with two different plane definitions, ring 1-7 (full plane) and ring 2-7 which excludes the inner ring of the trigger counters.

The first level ring 2-7 trigger has a rate of $2.4 \cdot 10^{-5}$ of the beam $\cdot \overline{\text{halo}}$ at 280 GeV, $1.7 \cdot 10^{-5}$ at 200 GeV, and $4.2 \cdot 10^{-6}$ at 120 GeV incident beam energy. The ring 1-7 trigger rate is about twenty times higher. These triggers require a minimum Q^2/Q^2_{max} respectively of 0.10 and 0.05.

The trigger rate is halved by requiring as a second level logic that the trigger is satisfied in either half of the detector (left, right). The reduction in trigger rate is mainly due to the elimination of some shower punch through and of soft halo muons which cross the axis of the detector with short oscillations.

The ring 2-7 trigger composition with 280, 200 and 120 GeV beam on a carbon target was typically: good events 14, 25 and 68%, hadronic punch through 80, 69 and 26%, and 6% halo at all three energies.

6. DATA ACQUISITION

6.1 On-line computers, Camac system and on-line control

The data acquisition of the experiment (fig. 13) is performed by a distributed hybrid system of a Hewlett-Packard 21MX-E computer with 160 K 16 bit words memory space and a Norsk Data NORD-10/50 computer system with 256 K 16 bit words memory each. The 21MX-E and the NORD-10 are equipped with standard peripherals (terminals, line printer, discs, magnetic tape

drives) and are both connected to a conventional CAMAC branch. They are interconnected via a bi-directional 300 Kbaud parallel link. The NORD-10 is also connected to the CERN Computer Center via the CERNET data communications network for transfer of data and program files, and to the INDEX terminal connections network for user access from remote terminals located anywhere on the CERN site.

The 21MX-E computer is dedicated exclusively to the data acquisition task. During the SPS beam spill, data are read from CAMAC on an event-by-event basis and stored into a 128 Kwords buffer. Data are subsequently recorded on 9-track 1600 bpi magnetic tape; tape writing is decoupled from data retrieval within the limit of the buffer size to minimize deadtime losses. At the end of each spill, counting rates from the experiment are recorded from CAMAC scalers and the status of the data acquisition CAMAC system is monitored. Important counting rates, global status information and any detected errors are logged on a system of TV displays. In between two successive spills a randomly selected sample of events is sent to the NORD-10 for monitoring purposes.

The software used is written in HP Assembler language and is based on the standard CERN data acquisition package for Hewlett-Packard computers [15]. Special software was developed to interface this package to the hardware configuration of the experiment, to drive the HP-NORD link, and to monitor and display the status of the acquisition system. The data acquisition software runs under control of a simple dedicated stand-alone operating system which employs the CERN-written BAMBI interpreter [16] as command processor and for communication with the user.

The root of the CAMAC system for data acquisition is a single standard EUR 4600 branch. To extend the system beyond the limit of 7 crates, and to minimize read-out deadtime due to software overheads, a number of autonomous CAMAC sub-systems is used which transfer data to buffer memories located in the main branch. Simple CAMAC modules like TDC's, coincidence registers etc. are read by a tree-structured ROMULUS read-only CAMAC system [17]. For each event, data are encoded from 56 320 MWPC channels, 560 trigger counter PMs and 500 beam hodoscope channels, together with all

relevant trigger information. Zero data from all non-hit experimental channels are suppressed at the CAMAC level. Consequently, only some 500 16-bit words are transferred to the computer and written to tape for one deep inelastic trigger. The corresponding deadtime is approximately 3 ms.

The NORD-10 computer monitors the performance of the experiment. It runs a commercially available multi-user time-sharing operating system which gives priority to real-time tasks but allows software development and execution of background jobs to proceed in parallel. Data flow through the real-time programs is controlled by the standard CERN software package for data acquisition on NORD computers [18].

The same computer also controls the setting of fast electronics located in the experimental area and monitors the MWPC high voltages via the SATAN experiment control system. For this purpose, the NORD-10 is connected to its own CAMAC branch via a system crate interface. Steering of the remote electronics proceeds via SATAN master controllers in this branch which in turn control via a slow serial loop the slave controllers attached directly to the electronics modules. All discriminator thresholds, timings and logic requirements are stored on a series of disc files, each of which corresponds to a specific trigger condition, and can be written into the SATAN controllers under program control. This allows to change pre-defined trigger conditions within a few seconds. The same programs allow to read all settings back into the computer and to visualize them conveniently on a number of status displays on a colour TV terminal. From the same terminal, the default settings stored on disc can be manually overridden any time. The actual status of the remote electronics is compared at regular intervals with the predefined settings as stored in the computer and any detected failures are reported.

The NORD-10, via a branch mixer, has also access to most crates of the data acquisition CAMAC branch. This is used for hardware tests outside data taking periods.

The main event reconstruction program of the experiment PATRAC [19] runs on the NORD-50 computer, either in standard off-line batch mode for mass production from tape or in on-line mode for complete real-time reconstruction of a sample of triggers. This computer does not have any peripheral devices of its own and all input/output proceeds via the NORD-10.

6.2 Data taking and on-line monitoring

The largest fraction of the running time is devoted to data taking with the DIS triggers described in sect. 5. In parallel, data are recorded for beam structure and normalization studies using an unbiased beam trigger defined by a coincidence between the standard beam signal and random pulses from a radioactive source. Upon this trigger, only the beam hodoscope information is recorded. Typically, about 100 deep inelastic events and the same number of beam events are collected for an effective spill of 1500 ms with 30% deadtime loss.

During data taking, the performance of all detectors in the apparatus is monitored with a system of FORTRAN programs on the NORD-10 computer which histograms continuously channel-by-channel and detector-by- detector fillings of all proportional chambers, trigger counters and beam hodoscopes, as well as time-of-flight distributions for the beam hodoscopes. Output signals from the higher-level trigger logic units are monitored in a similar fashion. All histograms are inspected visually at regular intervals, normally once in a few hours, and compared to reference plots. A graphic event display serves to study event topologies for different trigger conditions and allows the rapid detection of obvious malfunctioning during data taking.

A sample of the recorded events is processed at regular intervals on the NORD-50 computer to monitor detector and trigger logic efficiencies.

Scaler rates from all counters and coincidence rates are recorded after each spill and checked for stability as a function of time and beam intensity. The currents of all beam transport elements are regularly examined via a terminal connected to one of the SPS control computers and

compared to reference values. The beam positions upstream and downstream of the apparatus are monitored with a system of small MWPC's connected to the same computer. The fields of both the spectrometer magnet and the beam momentum station magnet are constantly measured with Hall probes connected to high precision digital voltmeters.

7. OFF LINE EVENT PROCESSING

7.1 Pattern recognition and track reconstruction

Most of the off-line analysis is performed in the framework of a single large program PATRAC [19] which includes the following steps:

(a) pattern recognition and event reconstruction,
(b) selection of DIS events,
(c) computation of detector efficiencies,
(d) computation of the incident muon flux and corrections for dead time losses.

The two main steps of the pattern recognition are the association of MWPCs hits into track segments, separately for the X and Y projections and the matching of these segments to get a 3-dimensional muon track pattern. The efficiency of the algorithm used was found to be 99.5%.

The fitting algorithm for momentum and scattering angle is based on the widely used "quintic spline model" [20], modified for the effect of finite energy loss along the track. Since the scattered muon becomes visible in the chambers only after traversing a few meters of iron, the fitted track is extrapolated back to the target by stepwise numerical integration of the equations of motion in the magnetic field, using as a boundary condition the results of the kinematic fit. In the target, the interaction vertex is defined as the point of closest approach to the track of the incoming muon as measured in the beam hodoscopes.

The selection of DIS events from the background which consists primarily of accidental halo tracks is performed with the help of the following criteria:

- track quality (at least four points in each projection and ten in the sum, mean MWPC and counter efficiencies along the track > 80%);

- that the track itself generates a trigger pattern consistent with the one recorded on PU and that the reconstructed half-ring hits match the experimental ones;

- kinematical cuts: the scattered muon momentum $p_\mu > 10$ GeV and Q^2 greater than a minimum value depending on the primary energy and trigger requirement.

Events which are not unambiguously identified as good or as background by the selection algorithm are flagged for visual scanning. The fraction of such events varies between 1 and 3 per cent of all reconstructed tracks, depending on beam energy and trigger conditions. Typically half of the scanned events are found to be good DIS. The misidentification of background events as good events and of good events as background was found to be less than 0.1% by scanning control samples of both categories. An example of a good DIS event is shown in fig. 14.

The redundancy of the trigger and the PU system allows to measure the MWPCs, TCs and overall trigger efficiencies directly from the DIS events. Typical efficiencies of the various components are: trigger counters $\sim$ 98%, logic stations $\sim$ 99%, and MWPCs $\sim$ 97%. These numbers refer to the overall performance of the apparatus and are therefore slightly lower than the efficiencies of individual detectors under test conditions (see section 4).

7.2 Determination of the incident flux

To calculate absolute cross sections, two different methods are used to evaluate the incoming muon flux and to correct for dead time losses. The first one consists in adding up the counts of all the scalers

corresponding to each individual cell of the beam defining hodoscope, after a small corrections for dead time losses (< 1%). The overall sum is then corrected for multiple hits (∿ 5%) and geometrical overlaps of the hodoscope cells (∿ 20%), the correction factor being determined in special low intensity runs and from the time correlation of the individual cells.

The second method of flux calculation uses a scaler which counts OR-ed pulses from the entire hodoscope but with a known dead time. The dead time correction (typically 20%) is evaluated statistically using the hodoscope TDC information. This method requires no corrections for multiple hits and geometrical overlaps of the hodoscope cells.

The two methods of flux determination always agree with each other within 1%.

7.3 Simulation of the experiment and experimental resolution

The Monte-Carlo simulation of the experiment is based on the program system GEANT, interfaced to the geometry of the spectrometer and to the physics of muon-nucleon deep inelastic scattering [21]. The program first generates incoming beam muons, traces them through the target and after the interaction traces the scattered muon through the apparatus. Tracking through the target and the spectrometer includes simulation of multiple scattering and energy loss including "catastrophic" losses from radiative and nuclear processes. Hits in detectors along the track due to hadronic and electromagnetic showers as observed experimentally have been parametrized and added to the MC simulation.

After applying the trigger conditions and all trigger and MWPC efficiencies as computed from experimental data, Monte-Carlo events are processes by the same reconstruction program as the data and are used to calculate the acceptance of the apparatus as a function of two kinematical variables, e.g. Q^2 and y (fig. 15). Inside the contours the acceptance is typically 80% for DIS events.

Simulated events have also been used to determine the resolution of the spectrometer. The momentum resolution is typically 8%, almost independent of the momentum itself but improving slightly with the number of measured points. This has been confirmed experimentally by steering beams of known momentum directly into the spectrometer magnet. The angular resolution is typically $\sim$ 3% and the resulting Q^2 resolution varies from 6 to 9% for focused muons where the momentum and angular errors tend to compensate each other.

8. CONCLUSIONS

The apparatus has operated with great reliability in all its components for over two years. A large sample of deep inelastic scattering events on carbon with incident energies of 120, 200 and 280 GeV has been accumulated. Some results on the nucleon structure functions have already been published [22] as well as an upper limit on the T production by muon beams [23].

The high statistics data at 120 and 200 GeV incident energies both with positive and negative muons are being analyzed to determine the asymmetry in the μ^+, μ^- cross sections as well as more precise values of the structure functions and of R, the ratio of the absorption cross section for longitudinally and transversally polarized photons.

ACKNOWLEDGEMENTS

The construction of this apparatus would be impossible without the support and constant encouragement of the directorates of CERN, JINR, and CEN. We also aknowledge the financial contribution of the Bundesministerium für Forschung und Technologie.

Many people in our home laboratories have devoted their skills and efforts to the planning, construction and commissioning of our equipment. In particular we would like to acknowledge the technical support of W. Birr, K. Bussman, V. Evdokimov, H. Herbert, S. Lazic and M. Shcherbakov and the EF Division at CERN. The magnet construction was possible thanks

to the contributions of V.L. Karpovsky, M.A. Liberman, G. Petrucci and of the JINR workshops. We would also like to acknowledge the invaluable help of E. Rimmer (on-line computing), G. von Holtey and N. Doble (muon beam), B. Danner and J.L. Perinet-Marquet (spectrometer magnet's power supply and cooling), D. Brahy, L. Pregernig, M. Rabany and E. Rossa (beam hodoscopes). Many physicists have contributed in the early stages of the construction and during their visits: T. Dobrowolski, A. Léveque, J. Maillard, I. Manno, J. Pilcher, D.D. Reeder, G. Smirnov, M. Spiro, P. Todorov, S. Vorozhtsov and J. Zsembery; to all of them we express our thanks.

The Dubna part of the collaboration is grateful to CERN for the continuous support and hospitality.

REFERENCES

[1] See e.g. R.E. Taylor in: Proc. 1975 Intern. Conf. on Lepton and photon interactions at high energies, ed. W.T. Kirk SLAC, Stanford, 1975, p. 679.

[2] E. Derman, Phys. Rev. D7 (1973) 2755;
N.N. Nikolaev et al. JETP LEH 18 (1973) 70.

[3] R. Cliff and N. Doble, CERN/EA/74-A.

[4] D. Brahy and E. Rossa, Les hodoscopes du spectrometre M2, SPS/EBP/Note 77-5;
D. Brahy and E. Rossa, High rate photomultiplier base and precise timing calibration, Nucl. Instr. & Meth. 158 (1979) 121.
L. Pregernig and M. Rabany, IEE Trans. on Nucl. Science , NS26, 717, 1979.

[5] O.C. Allkofer et al., Nucl. Instr. and Meth. 179 (1981) 445.

[6] L.M. Lederman and M.J. Tannenbaum, Advances in particle physics, vol. I, John Wiley, 1968, p.11.

[7] Ch. Iselin, HALO, a computer program to calculate muon halo, CERN 74-17 (1974)

[8] D. Bollini, et al. Proc. of the 1980 Int. Symp. on High Energy Physics with polarized beams and polarized targets (C. Joseph and J. Soffer eds.), Birkhäuser Verlag, 1981, p. 482;
D. Bollini, et al. Il Nuovo Cimento 63A (1981) 441 .

[9] J. Cvach et al., Czechoslov Journal of Phys. B31 (1981) 709.

[10] F6, Société pour l'étude et la fabrication de circuits intégrés spéciaux, notes technique No. 78069, 78070, mars 1978, Grenoble, France.

[11] PCOS II, Proportional chamber operating system, Le Croy Research Syst. Corp., Spring Valley, New York.

[12] A.V. Vishnevsky et al., JINR reports P13-10856, P13-10939, Dubna 1977.

[13] A. Benvenuti et al. Nucl. Instr. and Meth. 125 (1975) 447

[14] F. Nanni, NA4-Note July 1977 (unpublished).

[15] E.M. Rimmer, ZDAQ, CERN-DD 1978 (unpublished).

[17] P.J. Ponting, CERN-EP Electronics Note 80-01 (unpublished).

[18] A. Bogaerts et al., ZDAS, CERN-DD 1978 (unpublished).

[19] R. Brun, CERN-DD/EE/79-3, 1979.

[20] H. Wind, Nucl. Instr. & Meth. 115 (1974) 431;
H. Wind, Nucl. Instr. & Methd. 153 (1978) 195.

[21] R. Brun et al., CERN-DD/78-2, 1978;
R. Brun et al., CERN-DD/EE/78-1, 1978.

[22] D. Bollini et al., Phys. Lett. 104 (1981) 403.

[23] D. Bollini et al., to be published in Nucl. Phys.

FIGURE CAPTIONS

Fig. 1 Schematic view of the spectrometer (a) and the structure of one supermodule, (b)

Fig. 2 Principle of the Q^2 focusing spectrometer.

Fig. 3 Curves of equal P_T and equal θ_μ for DIS in the Q^2, y plane, with 280 GeV beam energy.

Fig. 4 The CERN SPS muon beam line (vertical layout): BH(V) is a horizontal (vertical) deflection, F(D) are focusing (defocusing) quadrupoles (a), layout of this apparatus (NA4) and the EMC detector (NA2) in the experimental hall EHN2 (b).

Fig. 5 Longitudinal polarization of the M2 muon beam in function of muon and pion energies.

Fig. 6 Detail of the MWPC structure.

Fig. 7 Schematic diagram of MWPC read-out electronics.

Fig. 8 MWPC efficiency as a function of the strobe delay obtained with 4.6 KV for two strobe widths, 100 ns (solid line) and 65 ns (dashed line).

Fig. 9 Details of the trigger counter structure.

Fig. 10 Structure of the beam hodoscopes.

Fig. 11 Schematic view of the halo wall.

Fig. 12 Layout of the distributed trigger.

Fig. 13 Block diagram of the data acquisition system.

Fig. 14 Computer reconstruction of a typical DIS event in the detector. Each rectangle represents one supermodule, the short lines inside each rectangle indicate the half ring hits in time with the event. (On the side view the half rings are drawn twice to reproduce the up - down ambiguity of the trigger counters). The small dashes under the side view indicate the trigger counter planes which gave hits in time with the event while the long dashes under the top view represent the logic stations that generated a trigger. The crosses are MWPC hits. The solid lines are the projections of the reconstructed track. Some kinematical variables are given under the picture.

Fig. 15 Contour of equal acceptance of the spectrometer for DIS events in the Q^2/Q^2_{max}-y plane at 120, 200, 280 GeV. Inside these contours the acceptance is larger than 40%.

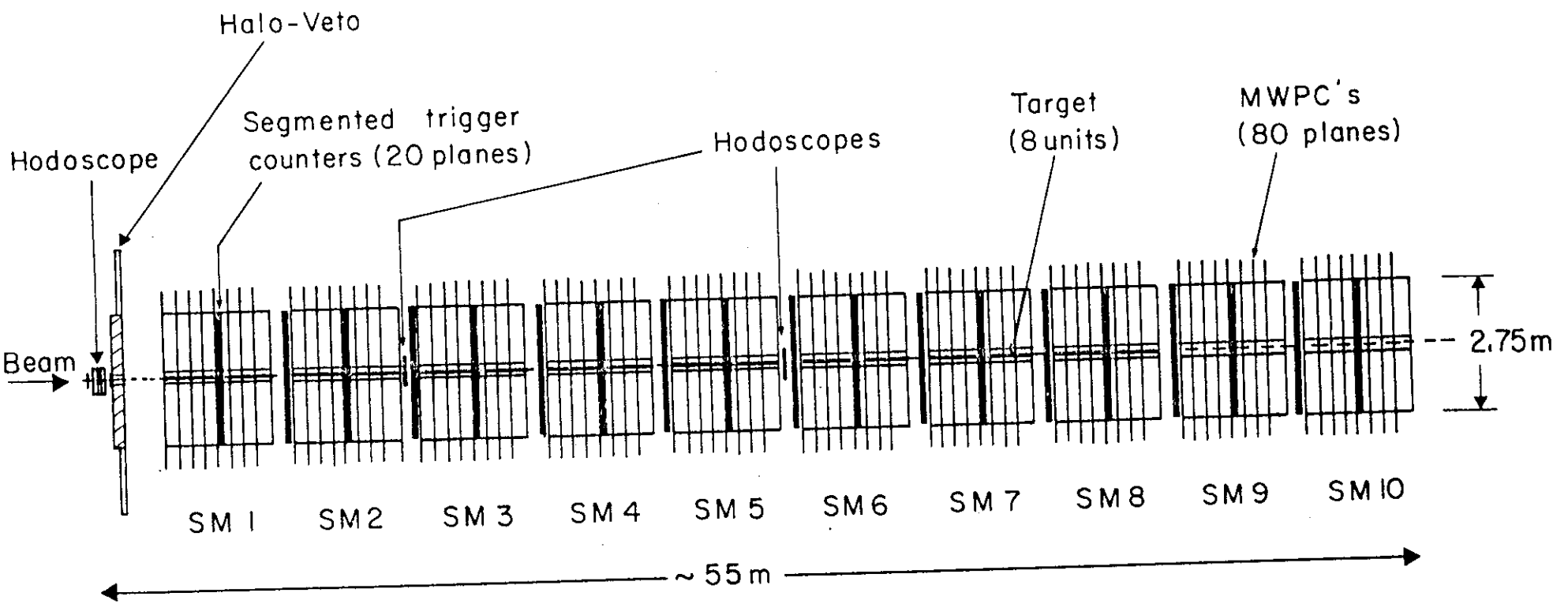
Halo-Veto
Hodoscope
Segmented trigger counters (20 planes)
Hodoscopes
Target (8 units)
MWPC's (80 planes)
Beam
2.75m
SM 1
SM 2
SM 3
SM 4
SM 5
SM 6
SM 7
SM 8
SM 9
SM 10
~55m

FIG. 1a

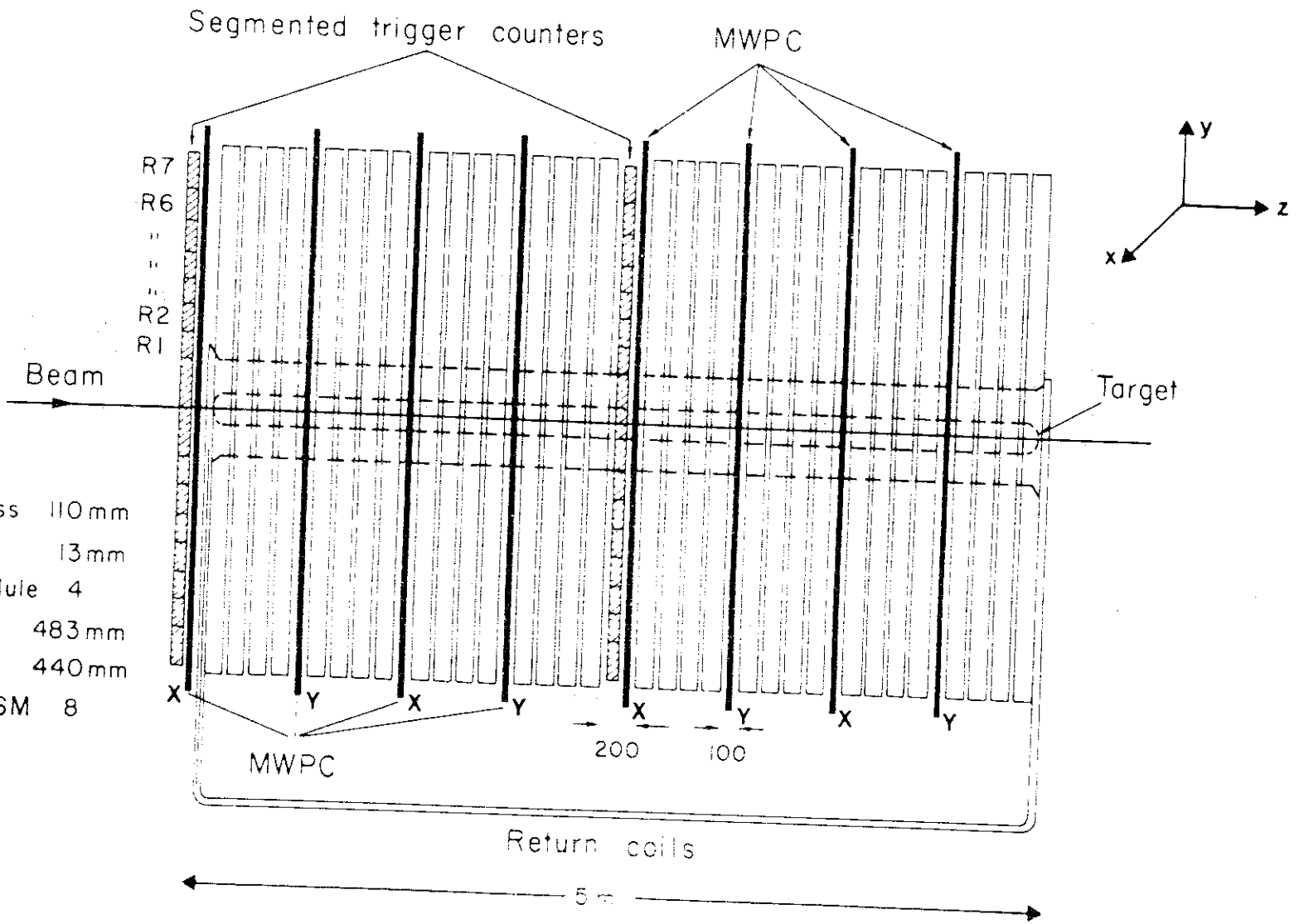

FIG. 1b

Plate thickness	110 mm
Gap	13 mm
N° plates / module	4
Length / module	483 mm
Iron / module	440 mm
N° of modules / SM	8

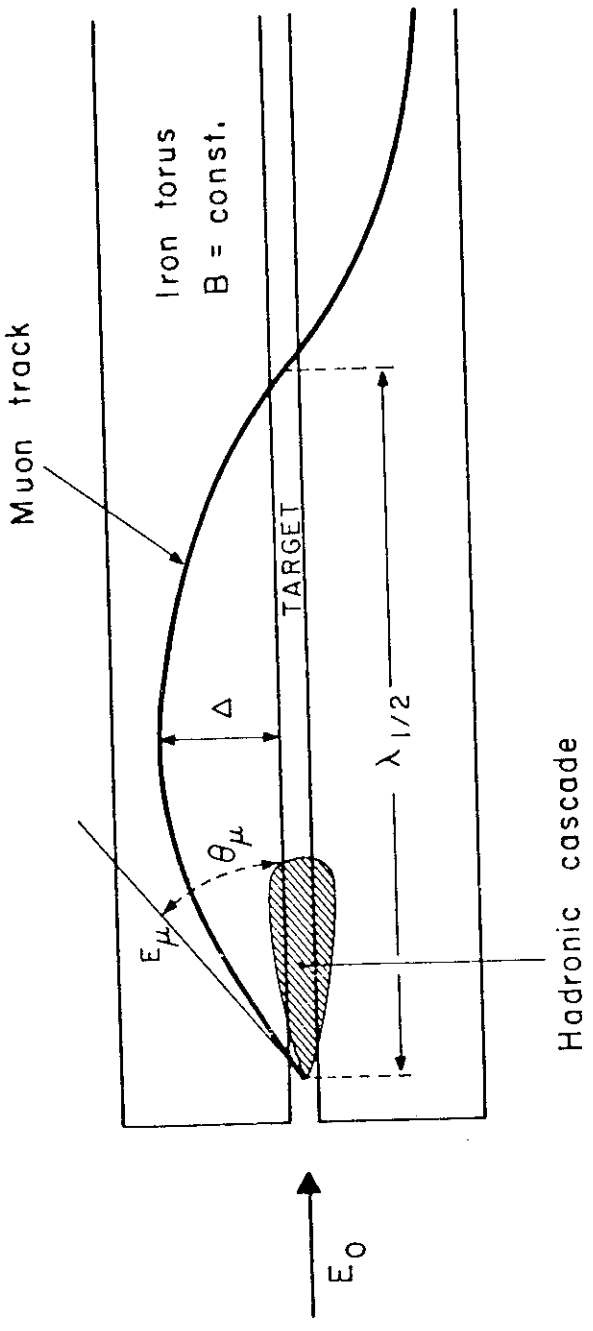

$$\lambda_{1/2} = 6.66\ p_T / B$$

$$\Delta = \frac{M}{0.3B} \cdot \frac{Q^2}{Q^2_{max}}$$

FIG. 2

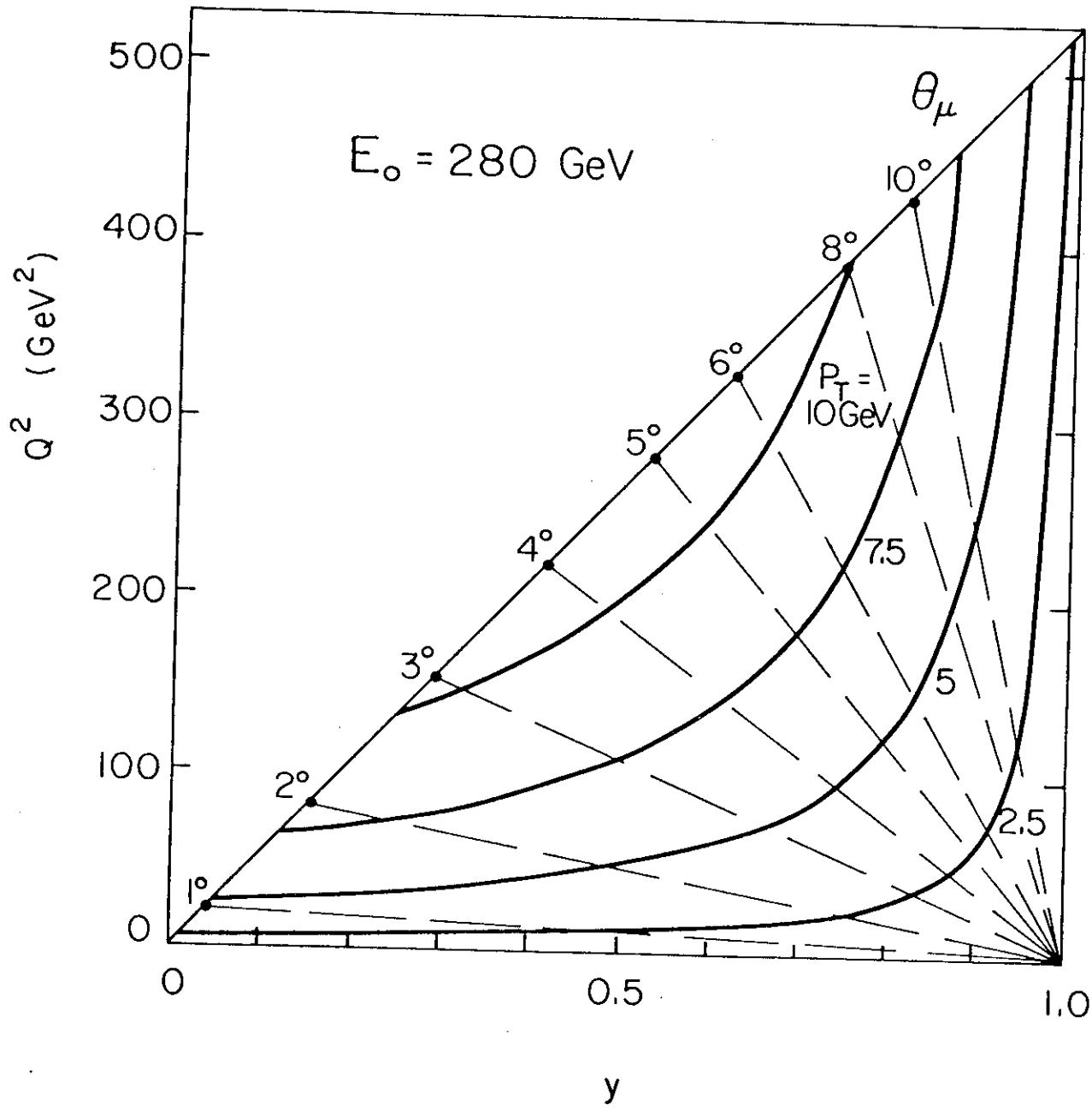
500
400
300
200
100
0
Q^2 (GeV^2)
E_o = 280 GeV
θ_μ
10°
8°
6°
5°
4°
3°
2°
1°
P_T = 10GeV
7.5
5
2.5
0
0.5
1.0
y

FIG. 3

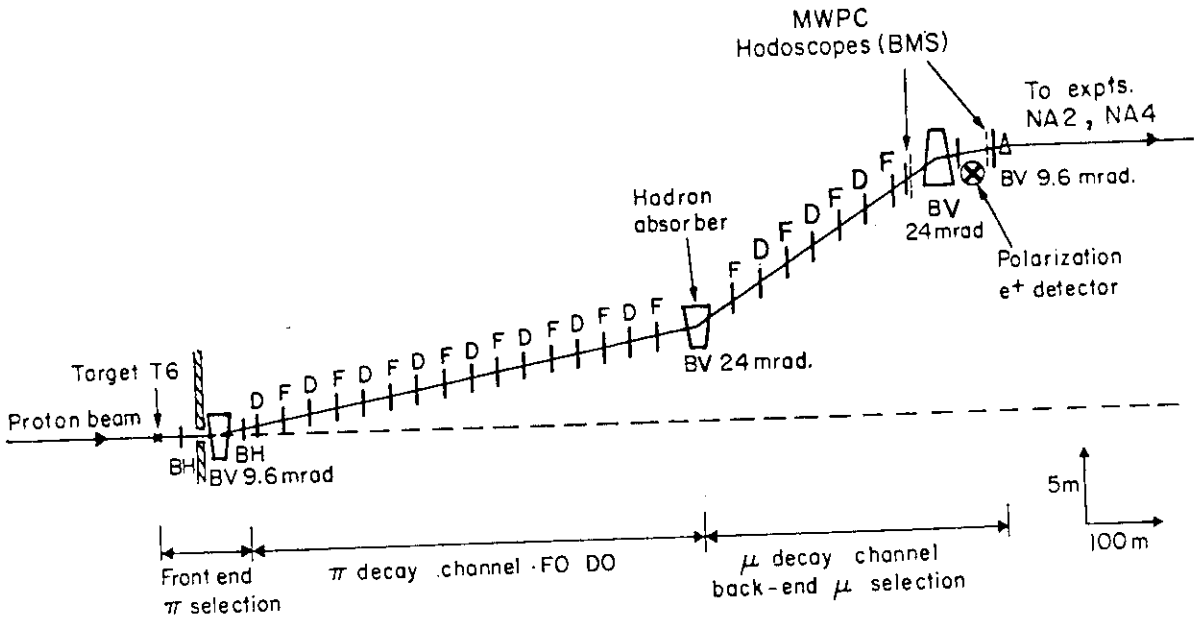
MWPC
Hodoscopes (BMS)
To expts.
NA2, NA4
BV 9.6 mrad.
Hadron
absorber
BV
24mrad
Polarization
e+ detector
BV 24 mrad.
Target T6
Proton beam
BH
BH
BV 9.6 mrad
5m
100m
Front end
π selection
π decay channel FO DO
μ decay channel
back-end μ selection

FIG. 4a

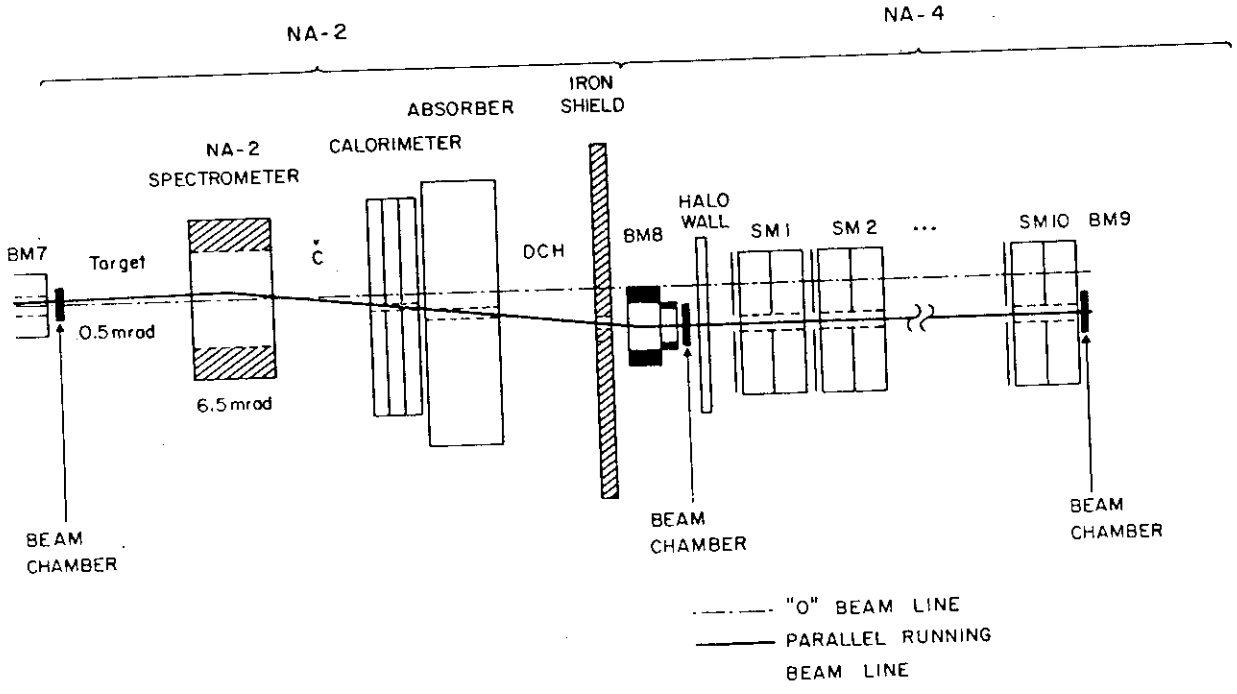
NA-2
NA-4
ABSORBER
IRON
SHIELD
NA-2
SPECTROMETER
CALORIMETER
BM7
Target
0.5mrad
6.5mrad
C
DCH
BM8
HALO
WALL
SM1
SM2
...
SM10
BM9
BEAM
CHAMBER
BEAM
CHAMBER
BEAM
CHAMBER
"O" BEAM LINE
PARALLEL RUNNING
BEAM LINE

FIG. 4b

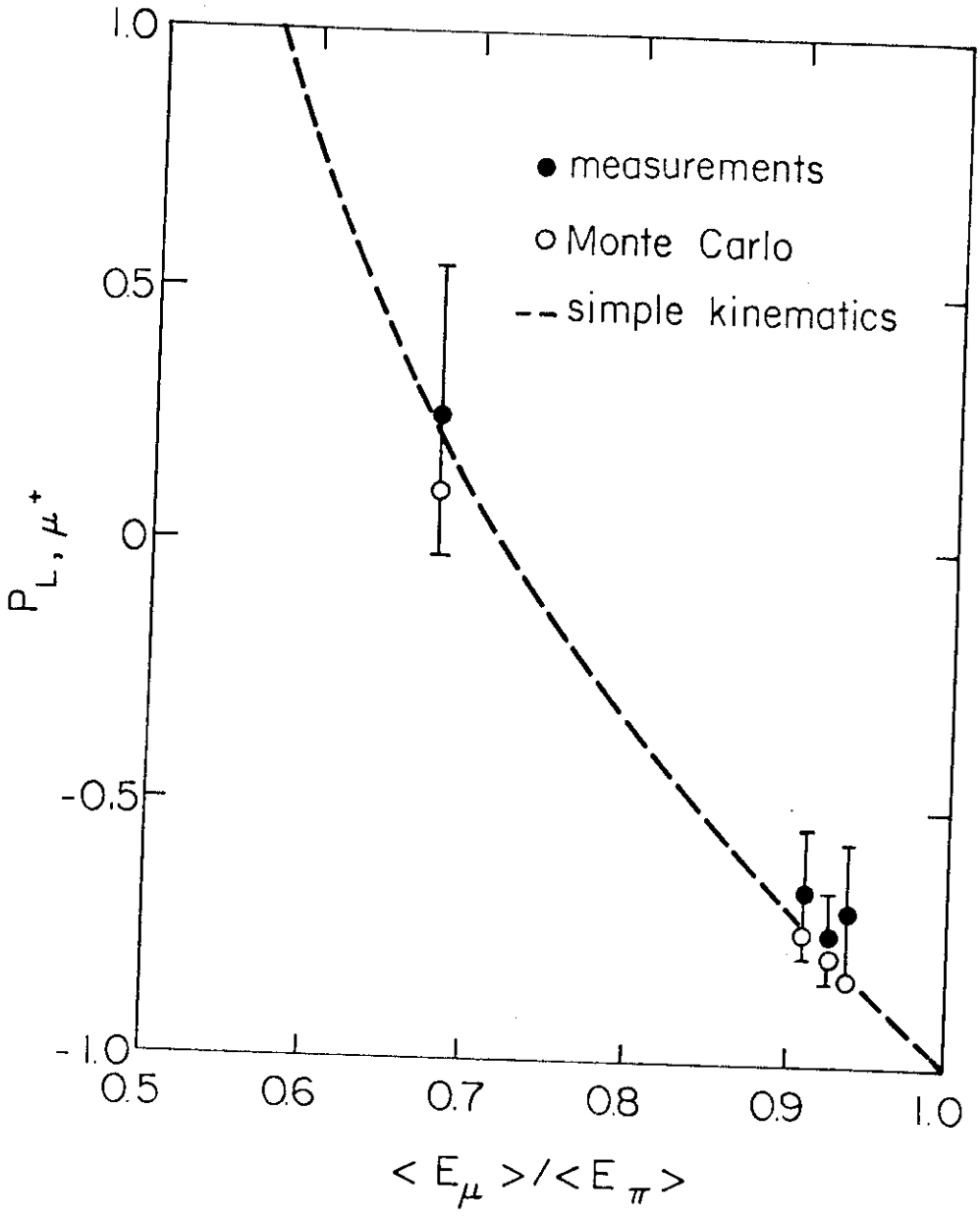
1.0
0.5
0
-0.5
-1.0
0.5
0.6
0.7
0.8
0.9
1.0
● measurements
○ Monte Carlo
-- simple kinematics
P_{L,μ^+}
$< E_\mu > / < E_\pi >$

FIG. 5

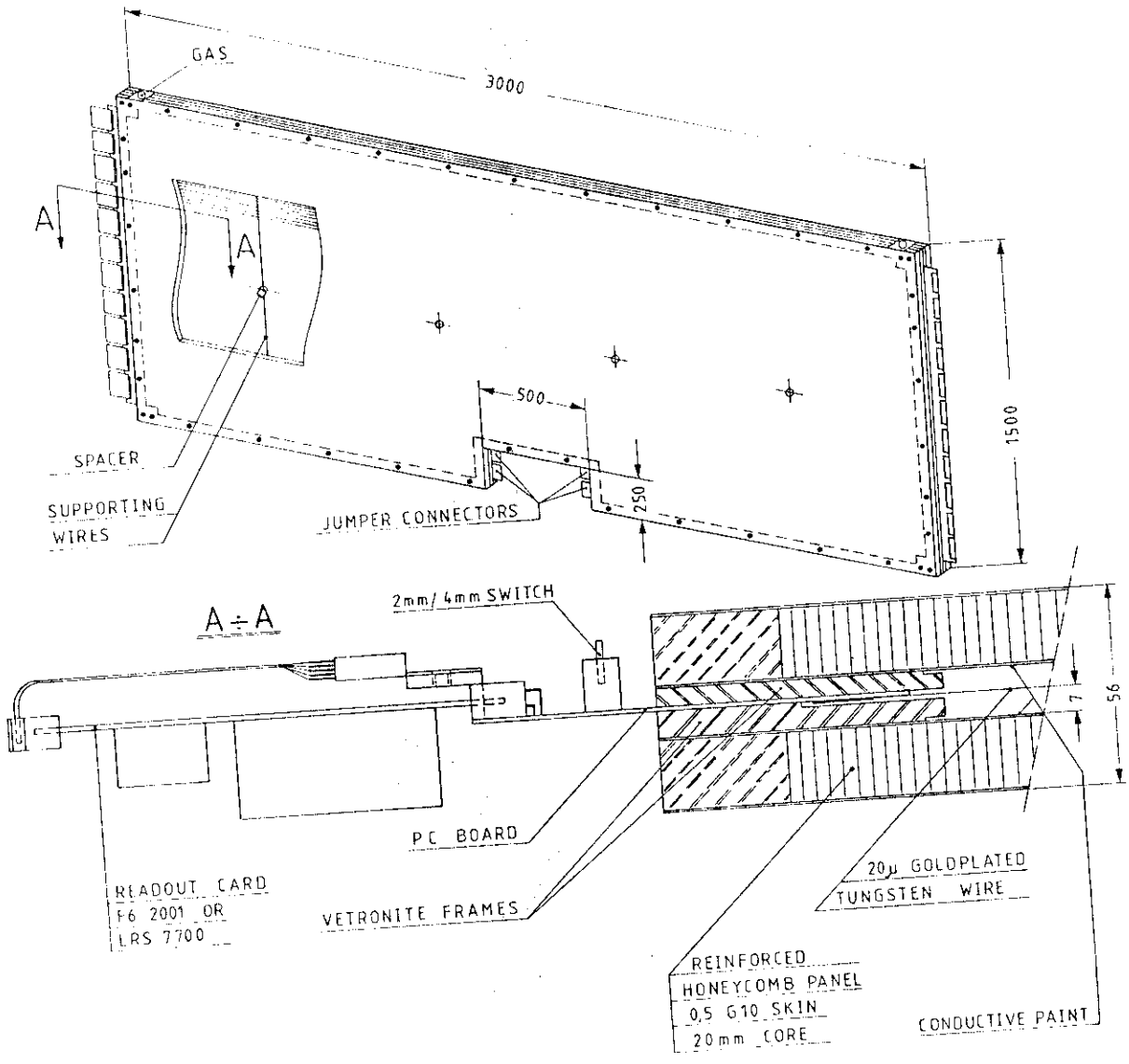
GAS
3000
A
A
500
1500
250
SPACER
SUPPORTING WIRES
JUMPER CONNECTORS
A÷A
2mm/4mm SWITCH
56
7
PC BOARD
READOUT CARD
F6 2001 OR
LRS 7700
VETRONITE FRAMES
20μ GOLDPLATED
TUNGSTEN WIRE
REINFORCED
HONEYCOMB PANEL
0,5 G10 SKIN
20mm CORE
CONDUCTIVE PAINT

Fig. 6

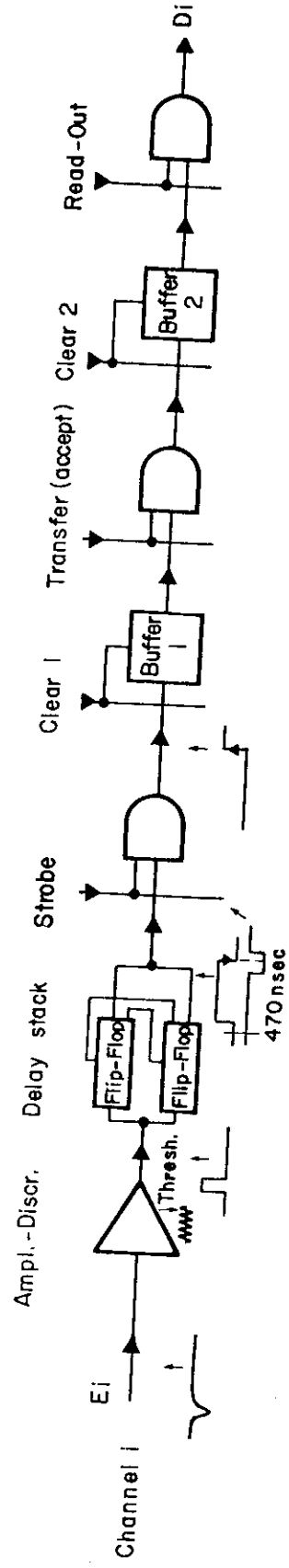
Channel i
Ei
Ampl.-Discr.
Thresh.
Delay stack
Flip-Flop
Flip-Flop
470 nsec
Strobe
Clear 1
Buffer 1
Transfer (accept)
Clear 2
Buffer 2
Read-Out
Di

Fig. 7

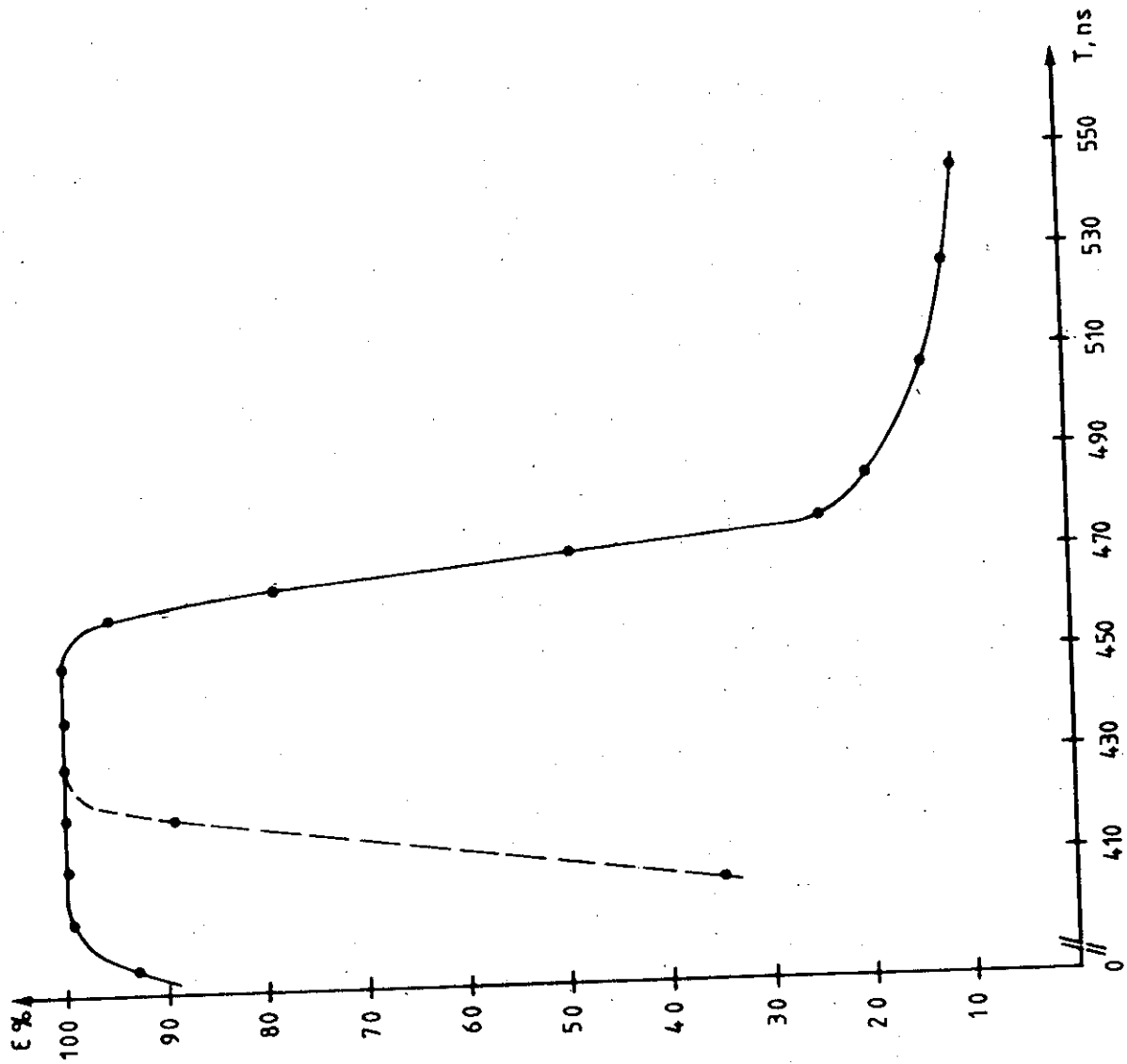
E %
100
90
80
70
60
50
40
30
20
10
0
410
430
450
470
490
510
530
550
T, ns

Fig. 8

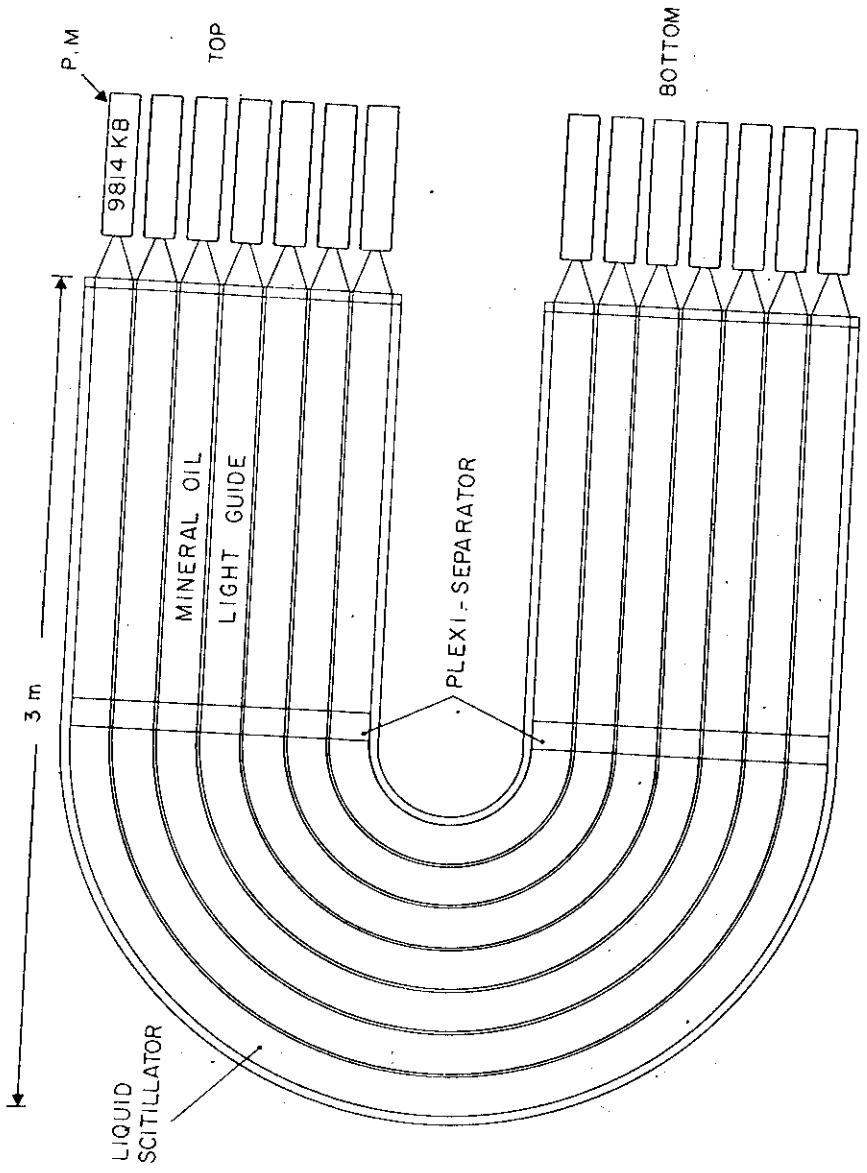
P.M
TOP
BOTTOM
9814 KB
MINERAL OIL
LIGHT GUIDE
PLEXI - SEPARATOR
3 m
LIQUID
SCITILLATOR

Fig. 9

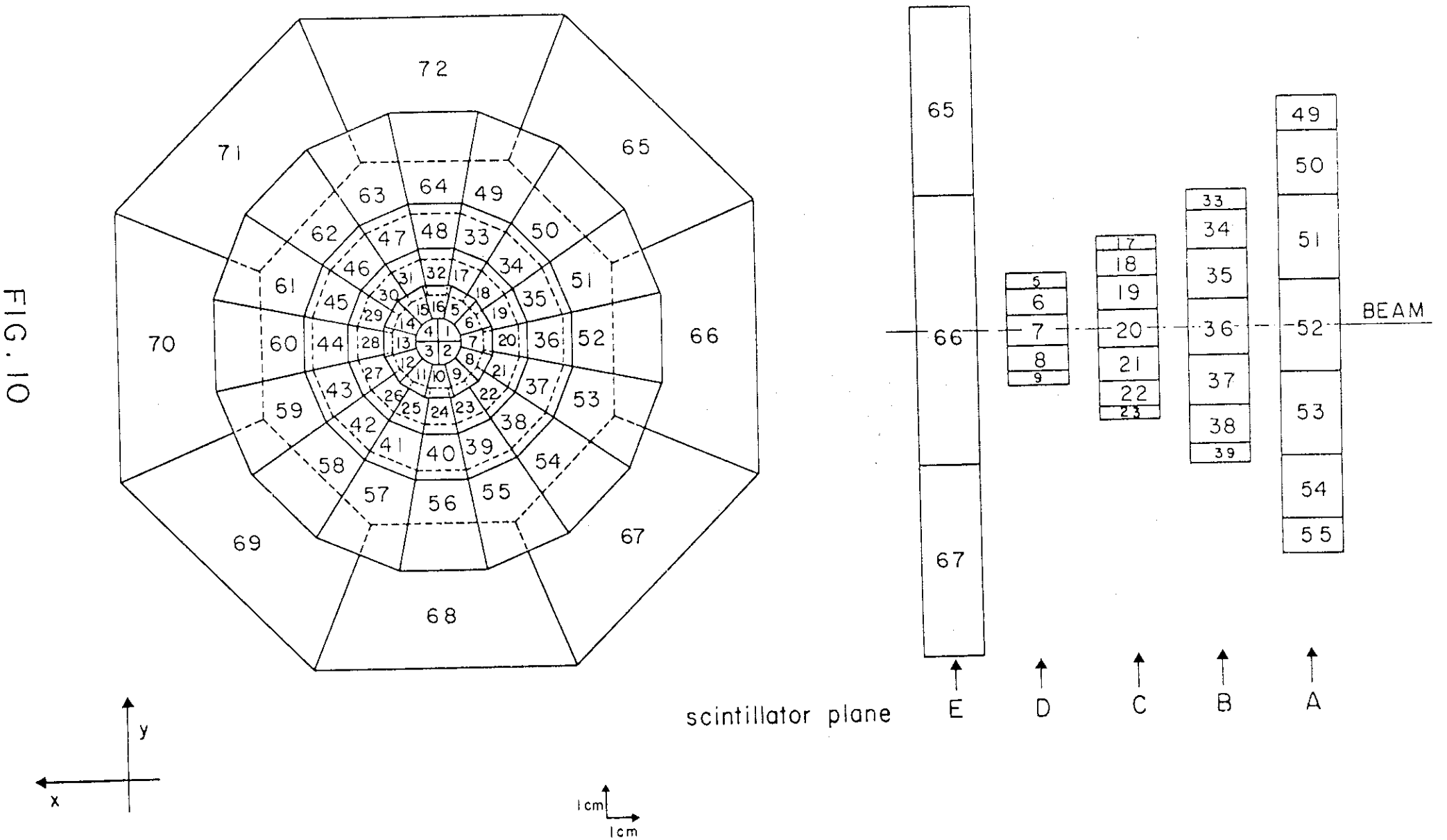
72
71
65
63
64
49
62
47
48
33
50
46
32
17
34
61
31
18
51
45
30
15
16
5
19
35
29
14
6
70
60
44
28
13
4
1
7
20
36
52
66
3
2
12
8
21
27
11
10
9
43
26
25
24
23
22
37
53
59
42
38
41
40
39
54
58
57
56
55
69
67
68
y
x
1cm
1cm
65
66
67
5
6
7
8
9
17
18
19
20
21
22
23
33
34
35
36
37
38
39
49
50
51
52
53
54
55
BEAM
scintillator plane
E
D
C
B
A

FIG. 10

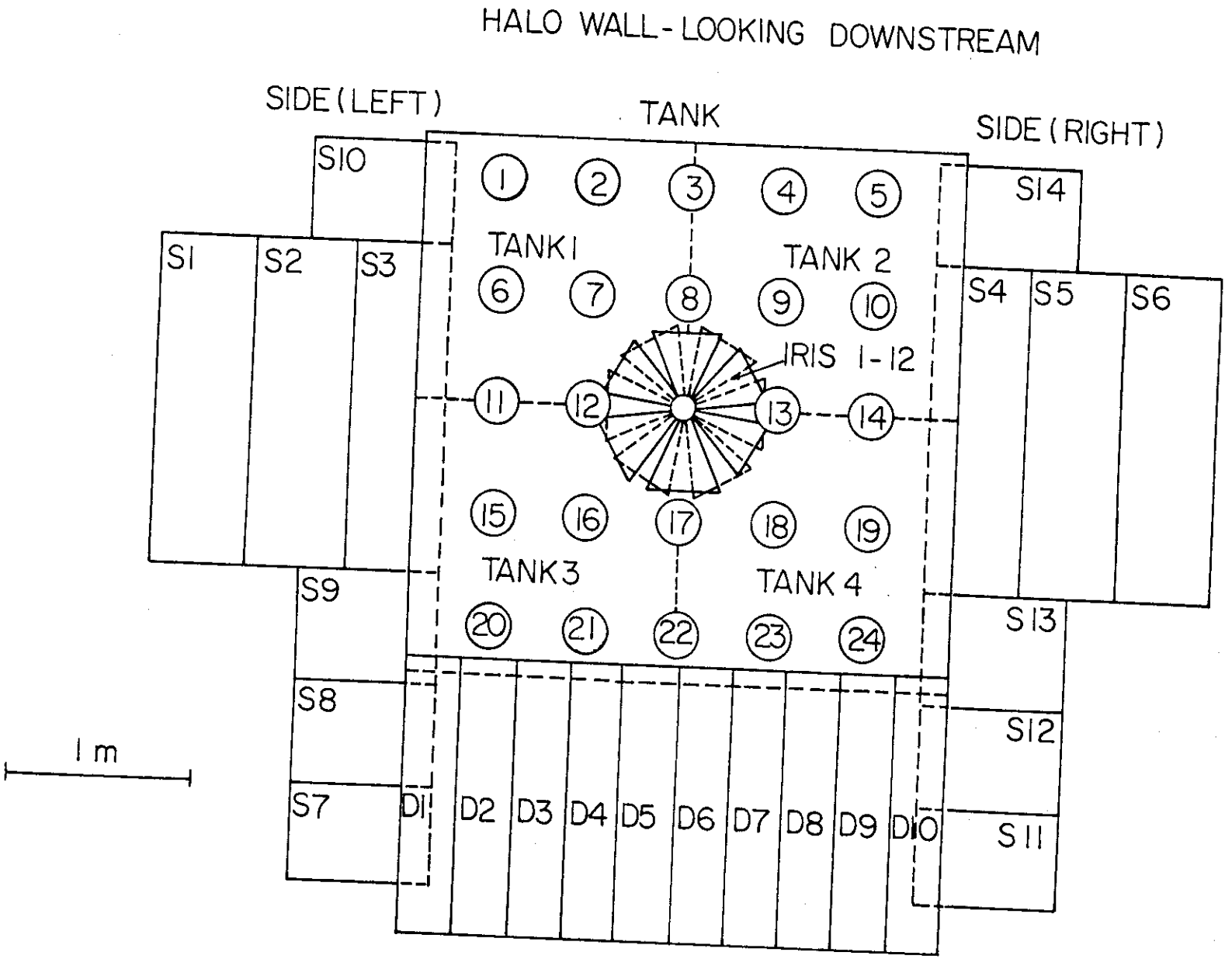
HALO WALL - LOOKING DOWNSTREAM
SIDE (LEFT)
TANK
SIDE (RIGHT)
S10
S14
S1
S2
S3
TANK 1
TANK 2
S4
S5
S6
IRIS 1-12
TANK 3
TANK 4
S9
S13
S8
S12
S7
S11
1 m
D1
D2
D3
D4
D5
D6
D7
D8
D9
D10

Fig. 11

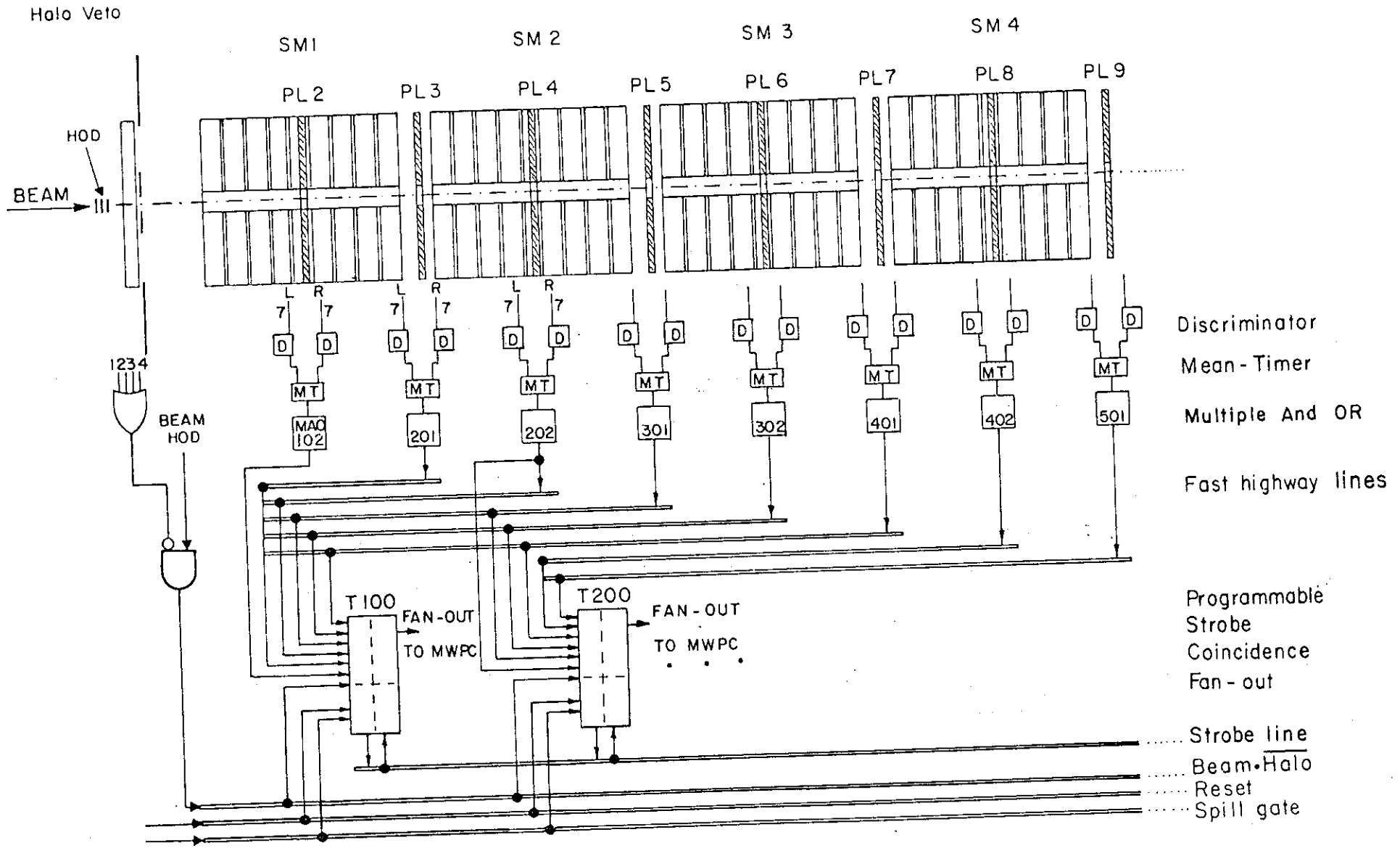
Halo Veto
SM1
SM 2
SM 3
SM 4
PL 2
PL 3
PL 4
PL 5
PL 6
PL 7
PL 8
PL 9
HOD
BEAM
1234
BEAM HOD
L
R
7
D
MT
MAO 102
201
202
301
302
401
402
501
T100
FAN-OUT
TO MWPC
T200
FAN-OUT
TO MWPC
Discriminator
Mean-Timer
Multiple And OR
Fast highway lines
Programmable Strobe Coincidence Fan-out
Strobe line
Beam•Halo
Reset
Spill gate

FIG. 12

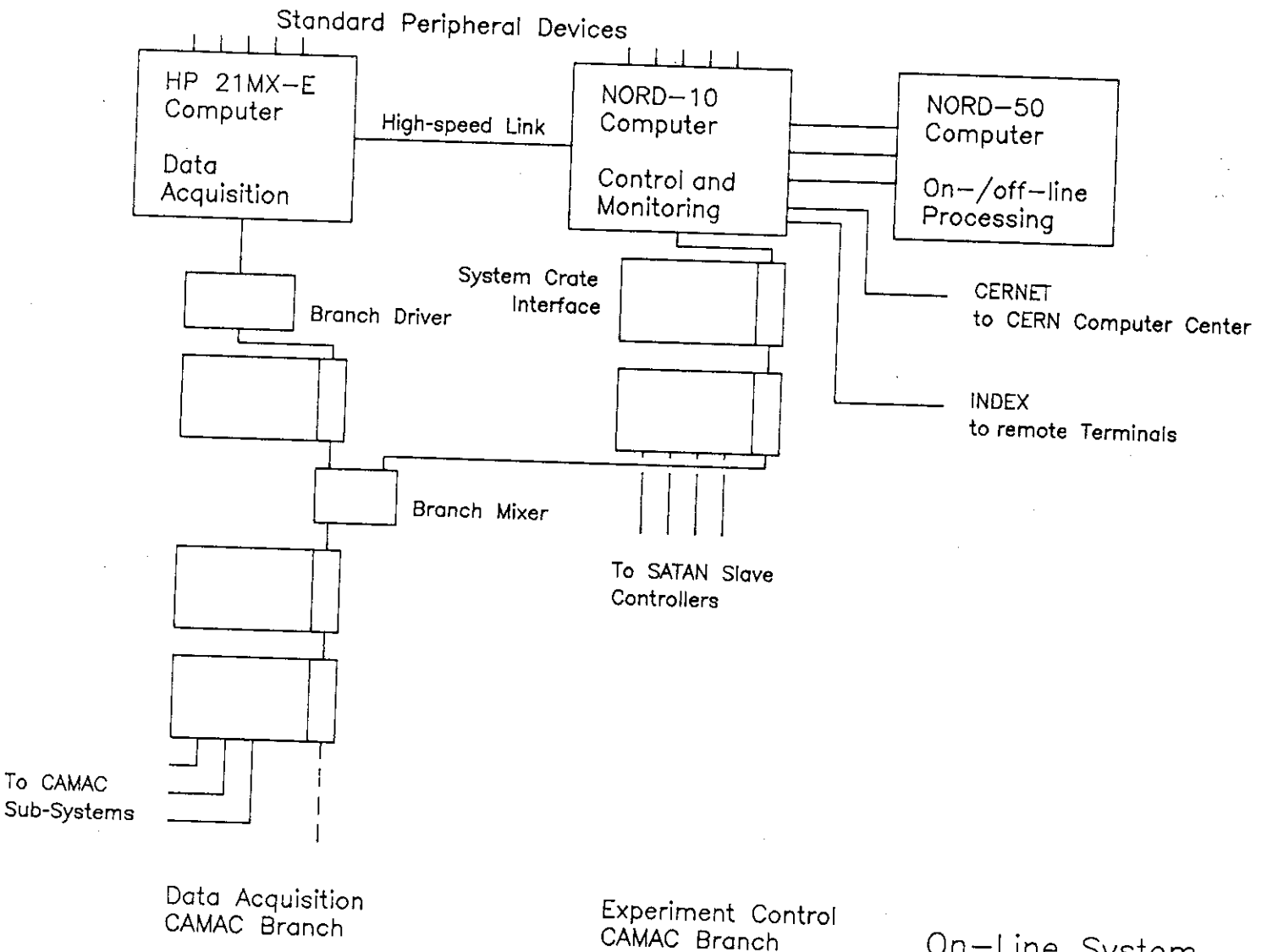
Standard Peripheral Devices
HP 21MX–E
Computer
Data
Acquisition
High-speed Link
NORD–10
Computer
Control and
Monitoring
NORD–50
Computer
On–/off–line
Processing
System Crate
Interface
Branch Driver
CERNET
to CERN Computer Center
INDEX
to remote Terminals
Branch Mixer
To SATAN Slave
Controllers
To CAMAC
Sub-Systems
Data Acquisition
CAMAC Branch
Experiment Control
CAMAC Branch
On–Line System

Fig. 13

Frame 3 Run 3628 Event 5682
Top View (x Projection)
Side View (y Projection)
Track
1
p (GeV/c)
– 46.82
Q² (GeV²)
169.391
ν (GeV)
144.5
x_Bj
.625

Fig. 14

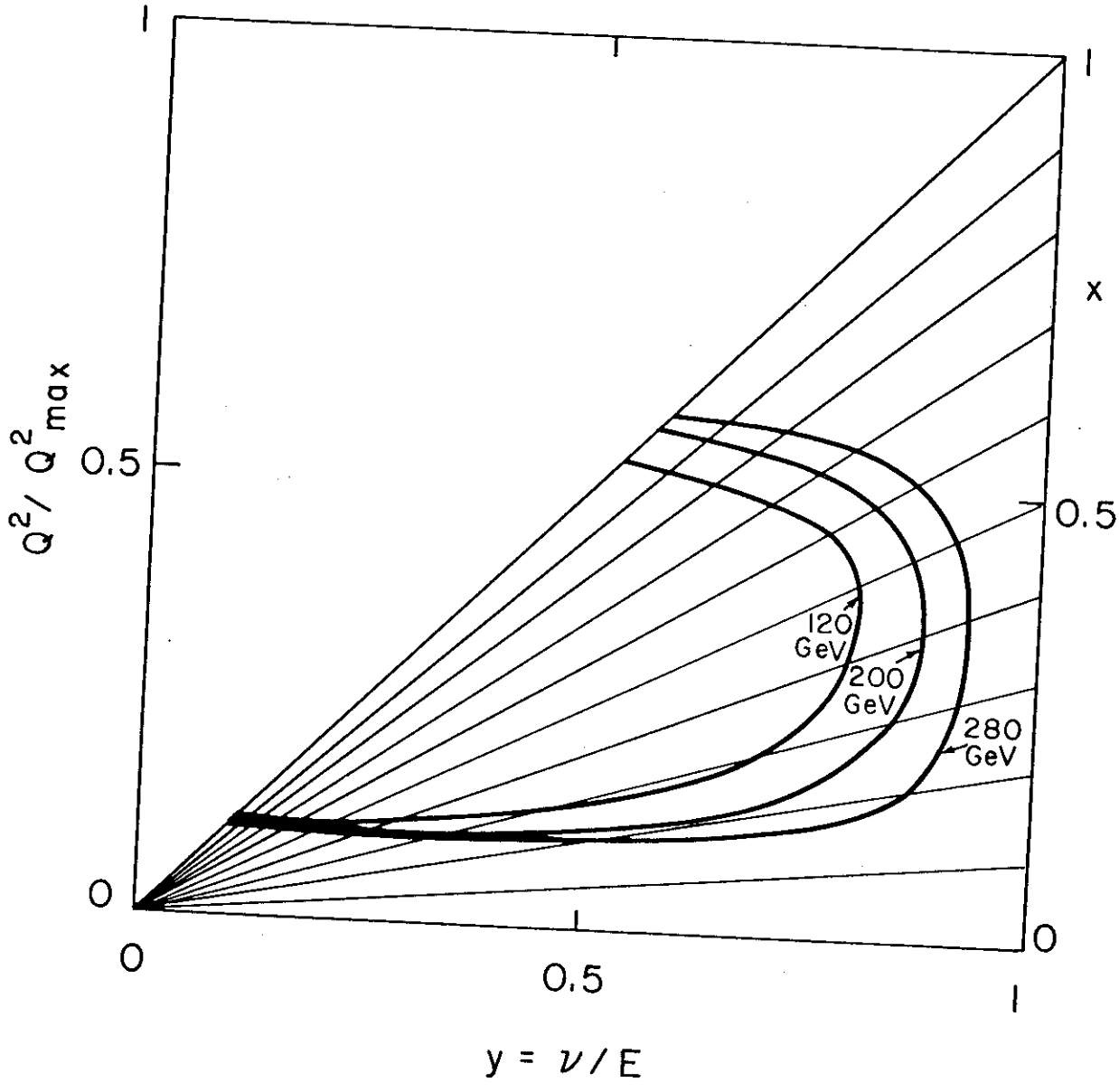

Fig. 15